Bubble behavior in a Taylor vortex

Rensheng Deng,[1,2] Chi-Hwa Wang,[2,3] and Kenneth A. Smith[1,2,*]
[1]*Department of Chemical Engineering, Massachusetts Institute of Technology, Cambridge, Massachusetts 02139, USA*
[2]*Singapore-MIT Alliance, 4 Engineering Drive 3, Singapore, 117576*
[3]*Department of Chemical & Biomolecular Engineering, National University of Singapore, 4 Engineering Drive 4, Singapore, 117576*
(Received 15 June 2005; published 7 March 2006)

We present a study on the behavior of air bubbles captured in a Taylor vortex formed in the annulus between two concentric cylinders. It is found that small bubbles stay either at certain locations near the vortex cores or in the outflow regions along the inner cylinder. If bubbles of the same size are introduced, a variety of bubble structures (such as ring, chain, cluster, etc.) appear due to different mechanisms. For bubbles of nonuniform size, orbit crossing of small and large bubbles is observed. Droplets and particles can also be captured in Taylor vortices, and these exhibit certain unique features.

DOI: 10.1103/PhysRevE.73.036306 PACS number(s): 47.55.D−, 47.32.C−, 47.55.Kf

Due to buoyancy, bubbles tend to rise to the top of a static liquid. However, if the fluid is contained between two vertical rotating cylinders, it is found that the bubbles may be indefinitely trapped. Moreover, if multiple bubbles are present, they may self-assemble into structures such as spirals, stripes, and rings [1–6]. In prior work, these structures were observed in the wavy vortex flow regime and the bubble size was quite polydisperse. A specific study on the behavior of individual bubbles, of pairs of bubbles, and of monodisperse groups of bubbles, in a nonwavy Taylor vortex has been unavailable, due partially to the constraints of traditional apparatus. The apparatus developed for this study has permitted observation of previously unreported phenomena.

The apparatus consists of a stationary outer cylinder (R_o =30 mm) and a rotating inner cylinder (R_i=18.4 mm) which provide a gap width (d=11.6 mm) sufficient for the development of various bubble structures. The working section length H is 60 mm, giving an aspect ratio $\Gamma=H/d=5.17$. A Newtonian mineral oil (with a density ρ of 0.86 g/cm^3 and a viscosity μ of 29.7 cp) was selected as the working liquid. Its high viscosity ensures laminar flow at rotational speeds (Ω) up to 800 rpm. A syringe pump drives air through a needle in order to generate uniform bubbles. The bubble size (d_b) is easily changed by altering the needle diameter. Bubbles can be injected at nearly any desired position with little perturbation to the flow from the needle itself. A high speed video camera working at a speed of 250/500 fps (frames per second) is employed to visualize the bubble behavior in the vortex. Both spatial and temporal information for bubble patterns can be obtained in this way.

We use a two-dimensional (2D) particle image velocimetry (PIV) system to monitor the liquid flow. Silver-coated hollow glass beads (d_p=14 μm) were adopted as the tracer particles. The position, shape, and velocity distribution of vortices can be determined [Fig. 1(a)]. It is found that a Taylor vortex first appears at a critical Reynolds number ($\mathrm{Re}_c=\Omega_c R_i d\rho/\mu$) of 62 and persists to at least a Reynolds number of 519. The observed critical Reynolds number is fully consistent with the prediction of Yim *et al.* for this radius ratio [7]. It should also be noted that the data show no sign of wavy vortices and this is consistent with the predictions of Edwards *et al.* [8] for low aspect ratio devices. As shown in Fig. 1(a), bubbles are of two kinds: one kind is found in the outflow regions along the inner cylinder ("wall bubble") and the other kind is found near the core of the Taylor vortex ("vortex bubble"). The former were reported by Shiomi *et al.* [1], but we believe that this is the first report of vortex bubbles which are arranged as a well structured "necklace."

To understand the nature of bubble capture, a computational fluid dynamics (CFD) software package (Fluent 6.1) was used to simulate the Taylor vortex flow. We are able to quantitatively reproduce the flow field observed in the experiments, as shown in Fig. 1(b). The experiments were performed by first establishing a steady state at Re=389 and then reducing the rotation rate to obtain the desired experimental value of Re. The simulation followed the same procedure, in an effort to model any hysteresis effects that might be present.

Figure 1(c) shows the calculated pressure distribution in the cross-sectional plane. At $P2$, there is a pressure minimum which corresponds to the outflow region where the wall bubble is found. This agrees with the expectation that the pressure force is responsible for the capture of wall bubbles [4]. However, a force analysis indicates that the pressure gradient cannot be responsible for the capture of a vortex bubble. Instead, fluid dynamic drag and the buoyancy force are the dominant terms in the force balance. In Fig. 1(c), the trajectory of a bubble released from $P1$ is predicted by the equations of motion contained within the particle tracking feature of Fluent. The principal forces are buoyancy and drag. Due to drag (and, to a lesser extent, the pressure gradient), it deviates from its initial motion and is gradually trapped in a Taylor vortex. However, because a velocity difference between the bubble and its neighboring liquid is needed to generate the required drag force, the bubble is not stable at the exact center of the vortex. Instead, it settles in a region of downflow, for example, to the right of $P3$ (denoted by the green circle), or to the left of $P4$ (denoted by the blue

*Electronic address: kas@mit.edu

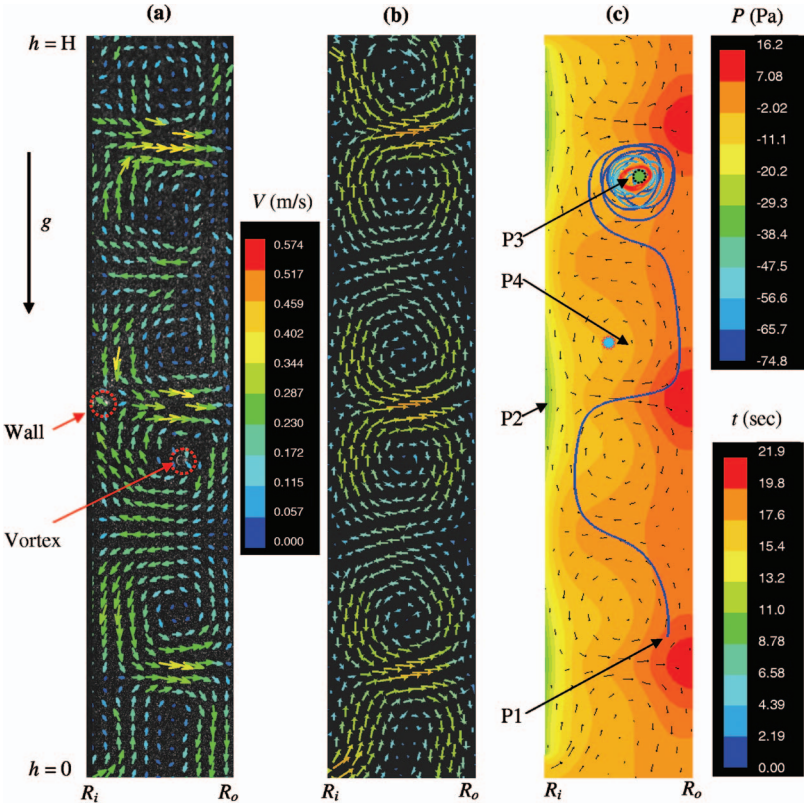

FIG. 1. (Color) Bubble captured in Taylor vortices (a) velocity field across the gap obtained from a 2D PIV system (Re=194) in the presence of both a vortex bubble and a wall bubble, as shown. g is the gravitational acceleration, h is the vertical position, R_i and R_o denote the radial positions of the inner and outer cylinder walls, respectively. (b) Velocity field calculated from Fluent simulation under the same conditions as (a). (c) Calculated contours of the pressure distribution corresponding to the velocity field in (b). The black arrows show the local velocity vectors, and the thick solid curve shows the trajectory of an air bubble (ξ=0.129) after being released from $P1$. The color bar between (a) and (b) shows the common velocity scale (m/s) for both (a) and (b), and the upper and lower color bars on the right side show the relative pressure scale (Pa) and tracking time (sec) for (c), respectively. $P2$, $P3$, and $P4$ correspond to the positions of the local pressure minimum, the core of a clockwise Taylor vortex and the core of an anticlockwise Taylor vortex, respectively.

circle). The larger the bubble size, the further it deviates from the vortex center. Furthermore, the diameter of the bubble orbit alternates from one vortex to the next ($P3$ to $P4$) and this was observed experimentally. For this reason, it is necessary to distinguish between these two types of vortex bubbles: those located between the inner cylinder and the vortex center are termed "*ic*"-vortex bubbles and those located between the outer cylinder and the vortex center are "*oc*"-vortex bubbles. Their differences will be addressed later. A detailed study also suggests that the release velocity and position significantly affect the result of bubble capture, as observed in the experiments.

Addition of single-size wall bubbles results in the formation of a chain structure, as shown in Fig. 2(a). The mechanism for the chain generation is unknown. Furthermore, such chains are found to be stable only at low Ω values and small bubble numbers (N), otherwise adjacent bubbles can coalesce into large bubbles and break the structure. This is different from the spiral/ring streak line observed by Shiomi *et al.* where the bubbles do not coalesce [1].

When bubbles of the same size are trapped in the interior of a certain vortex, a bubble ring forms in the annulus such that bubbles are azimuthally uniformly distributed, as shown in Fig. 2(b). This uniformity is quite astonishing because the second bubble may well be 50 bubble diameters removed from the first. The ring circulates at a speed ω along the annulus in the same direction as the inner cylinder. The formation of a regular bubble ring can be described as follows. For a N-bubble ring, the newly introduced $(N+1)$th bubble gradually approaches the equilibrium position along a trajectory such as the simulated one shown in Fig. 1(c). Finally, the bubble settles in between two adjacent bubbles in the ring. Then, the distance between adjacent bubbles rearranges during an "azimuthal adjustment" until the bubbles are uniformly distributed in the new $(N+1)$ ring. The whole procedure may be quite slow. For example, it takes approximately 80 min for a two-bubble system (Re=194, d_p=0.9 mm) to evolve from an initial distribution (in which the azimuthal separation between the two bubbles is 24°) to the equilibrium structure (with a separation of 180°).

For large values of N, the newcomer cannot easily enter the necklace. The newcomer therefore "invites" a bubble already in the ring to join it in a pairing such that each follows a corkscrew-like trajectory until nearby bubbles have made room for them to assume their desired positions. However, there is a saturation number, N_s, beyond which the above bubble-addition process cannot continue. In the state of saturation, the newcomer will not settle down, even after a long time (experimentally we wait for 1 h); and it finally coalesces with its "partner" (and, sometimes, with several other nearby bubbles) in the ring to form a single large bubble. Thus the ring is no longer uniform in bubble size. The newly formed large bubble may escape from the orbit and disappear at the liquid surface, in which case the remaining bubbles reorganize and form a regular ring structure once again. Alternatively the new bubble may not be large enough to escape and a ring composed of the original small bubbles and one large bubble persists.

As shown in Fig. 3, for the same bubble size, N_s increases with increasing Reynolds number. Also, but not shown, it is found that a smaller bubble size corresponds to a higher N_s value. For example, at Re=194, N_s increases from 71 to 150 when bubble size ($\xi=d_b/d$) decreases from 0.152 to 0.068. At "saturation," the bubbles are quite closely packed in the

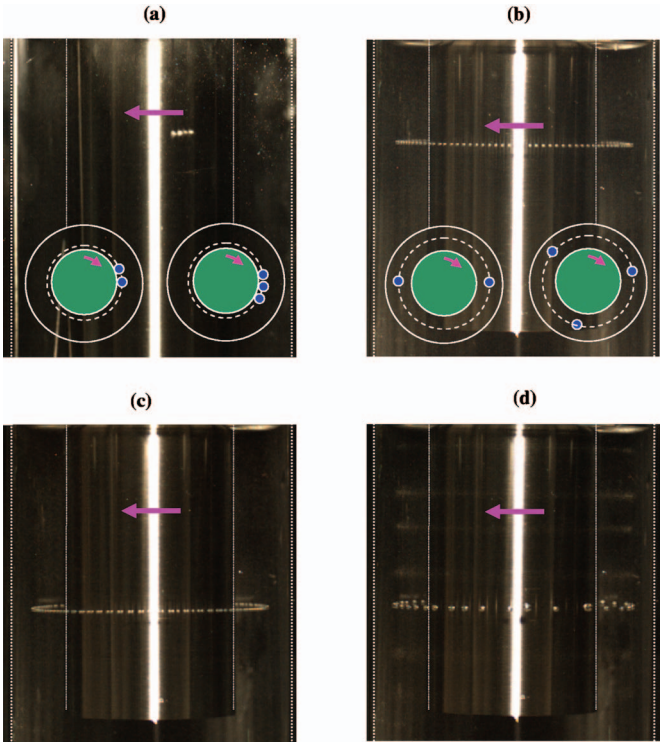

FIG. 2. (Color) Typical bubble structures recorded by the high-speed video camera (a) a 4-bubble chain of wall bubbles; (b) a 110-bubble ring of vortex bubbles. The two subpanels in (a) and (b) show the schematic top view of a chain/ring with two and three bubbles, respectively. (c) and (d) show the evolution of a clustering ring into one with larger, but fewer, bubbles, with (d) being photographed 30 min later than (c). The white stripe on the inner cylinder is the reflection due to the illumination while the thin and thick dotted lines are inserted to delineate the inner cylinder wall and the inner wall of the outer cylinder, respectively.

annulus. For instance, with $d_b=1.76$ mm and $N_s=71$, $Nd_b/2\pi R_r=0.76$. For $d_b=0.8$ mm and $N_s=150$, $Nd_b/2\pi R_r=0.75$. Here R_r is the radius of the bubble ring. This extremely dense packing is consistent with our observation of ring breakage shown in Fig. 2(c): the newly introduced bubble can settle down after radial and azimuthal adjustments but, if the distance between adjacent bubbles is very close, many small clusters form—usually composed of two or three bubbles. These small clusters then coalesce into large bubbles; however, because the size of the new bubbles may still not be large enough to permit escape from the orbit, the original ring of small bubbles can evolve into a ring of larger bubbles [Fig. 2(d)]. Note that bubble size in the new ring is not uniform because different clusters may contain slightly different numbers of bubbles.

From the above, we can see that bubble coalescence and escape are key factors in the stability of bubble structures; thus it is important to determine the maximum bubble size captured in a certain orbit. As shown in Fig. 3, for each operating speed, there is a maximum bubble size ξ_m beyond which the bubble escapes. The whole dataset from experiments and simulation can be best fit with a power function, showing that ξ_m is solely dependent on the square root of the relative Reynolds number (Re-Re$_c$). To characterize this feature, we developed a simple model by assuming that the bubbles of the maximum size escape from the location with the maximum downward fluid velocity (V_{am}). From a Fluent simulation of the short column used in this study, V_{am} was found to be nearly proportional to the difference between the actual speed of the inner cylinder and the speed at the onset of Taylor vortex flow, i.e.

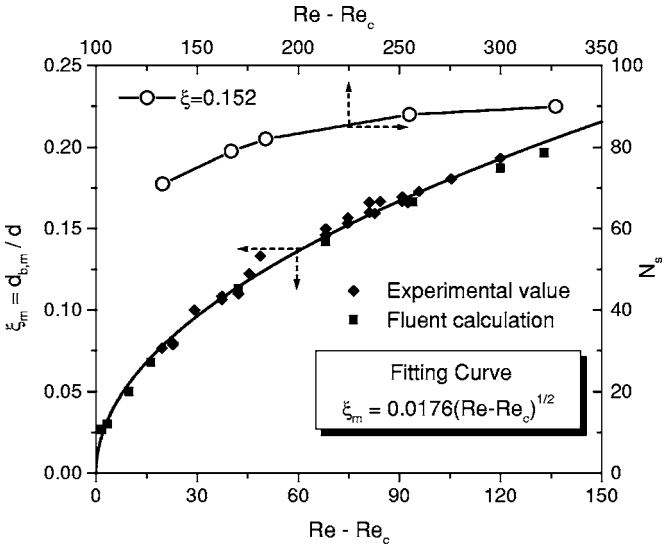

FIG. 3. Maximum bubble size, $d_{b,m}$, and saturation number, N_s, for *oc*-vortex bubbles captured at certain Reynolds numbers. The gap width, d, is used to form a dimensionless bubble size, ξ_m. The diamonds and squares show the maximum bubble sizes obtained from experiments and Fluent calculation, respectively. The open circles show the dependence of the saturation number on the Reynolds number. The curve for the maximum bubble size is the best fit for all the data points.

$$V_{am} = KR_i(\Omega - \Omega_c) \tag{1}$$

with $K \approx 0.184$. This result is different from that obtained by Davey [9] for an infinite aspect ratio. If the drag force balances gravity and if Stokes' law applies, we obtain

$$\xi_m = \sqrt{\frac{18K\mu^2}{\Delta\rho d^3 g\rho}}(\text{Re-Re}_c)^{1/2} = C(\text{Re-Re}_c)^{1/2}. \tag{2}$$

The coefficient C is estimated to be 0.016. This differs from the experimental correlation by 8.5% and is therefore in good agreement. The difference between the model and the data is not due to any small uncertainties in the latter, but rather to the simplicity of the model. The model also indicates that both *ic*- and *oc*-vortex bubbles have nearly the same maximum size at a given Reynolds number, which is confirmed by the experimental observations.

Another parameter which characterizes the bubble ring/chain is its angular speed. As shown in Fig. 4, the nondimensional speed ϖ is independent of the number of bubbles in the ring/chain. For a single wall bubble, ϖ decreases with increasing bubble size but is almost independent of Re. For example, it is equal to 0.91 for $\xi=0.112$, which may imply some kind of "rolling" motion between the bubble and the inner cylinder. For vortex bubbles, however, ϖ depends on

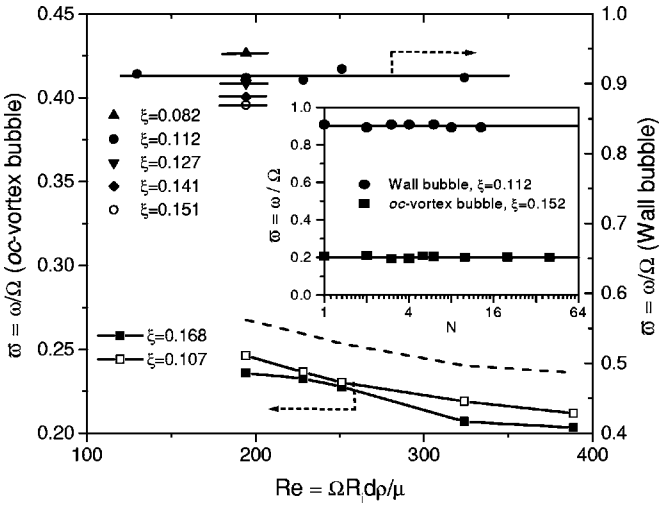

FIG. 4. Circulating speed of ring/chain at various bubble numbers (N) and Reynolds numbers (Re). The squares denote the circulating speed of rings composed of *oc*-vortex bubbles and other symbols denote the circulating speed of chains composed of wall bubbles. The dashed curve shows the undisturbed liquid speed at the vortex center obtained from simulation.

whether the bubble is of the *oc* or the *ic* type. For instance, at Re=389 and ξ=0.155, ϖ_{oc}/ϖ_c=0.86 and ϖ_{ic}/ϖ_c=1.01, where ϖ_c is the undisturbed liquid velocity at the center of the vortex. Figure 4 shows that ϖ decreases as speed increases; and small bubbles move faster than large bubbles. The dependence of ϖ on ξ leads one to wonder what might happen if two bubbles with different sizes were to travel nearly the same orbit. Taking an *oc*-vortex bubble as an example, it is observed that the smaller bubble (BS), having a higher circulating speed as stated above, soon catches up with the large bubble (BL). Because BS holds a slightly lower, but outer, position than does BL (the displacement may be less than d_b), it overpasses BL by steering below it and moves ahead, followed by successive chasing-overpassing games. The larger the difference in bubble size, the more easily they overpass. However, overpassing is a dangerous process for the two bubbles during which they might coalesce into one bubble, especially at high rotation speeds. Even if they can survive for a time, the crossing behavior does not continue indefinitely; the difference in circulating speeds becomes less and less significant due to the mutual interaction between the two bubbles, until finally a state is reached in which they coalesce to form a ring of nonuniform bubbles, much like that shown in Fig. 2(d).

By analogy, droplets (water, ρ=1.0 g/cm^3) and solid particles (glass beads, ρ=2.5 g/cm^3) might be expected to behave much like bubbles, although they tend to sink, rather than float, in the mineral oil. It is observed that the droplets/particles exhibit a "dancing" behavior at high rotation speeds: they exhibit a characteristic periodic oscillation in the axial, radial and tangential directions. Such a motion can be viewed as a combination of the particle motion in the vortex flow and along the annulus, although it is very much complicated by the unmatched periods of the two motions. This behavior has been explored by Wereley and Lueptow in the absence of gravity [10]. We find that gravity actually has a significant influence. As a result, the observed limit cycle for the dancing particles is not centered on the vortex, as in the results of Wereley and Lueptow [10], but is instead offset so that particles reside mostly in regions of upflow. Such a "dancing" behavior becomes less significant with decreasing rotational speed until finally the trajectory is purely azimuthal, and the equilibrium position is always lower than the position of the vortex core. Both droplets and particles can form rings, but the mechanism for ring breakage is different from that for bubbles; without coalescence, one droplet/particle falls out of the orbit if it is too close to another.

In summary, we have presented a set of complicated bubble (and droplet/particle) behaviors observed in a seemingly "simple" Taylor vortex system, including the different radial positions of *ic* and *oc* bubbles, uniform spacing between bubbles of the same size within a planar group of bubbles, orbit crossing of small and large bubbles, and "dancing" of particles. The capture of vortex bubbles in a Taylor vortex can be satisfactorily explained by the balance of drag force and gravity in the vertical direction. When bubbles are azimuthally, or nearly azimuthally, distributed, as in rings or in passing events, the interactions are not well understood. These phenomena are to be the subject of further study.

This work was supported by grants from the National University of Singapore, Singapore-MIT Alliance, and Massachusetts Institute of Technology.

[1] Y. Shiomi, H. Kutsuna, K. Akagawa, and M. Ozawa, Nucl. Eng. Des. **141**, 27 (1993).
[2] H. Djeridi, J.-F. Fave, J.-Y. Billard, and D. H. Fruman, Exp. Fluids **26**, 233 (1999).
[3] K. Atkhen, J. Fontaine, J. L. Aider, and J. E. Wesfreid, C. R. Acad. Sci., Ser. IIb Mec. **327**, 207 (1999).
[4] K. Atkhen, J. Fontaine, and J. E. Wesfreid, J. Fluid Mech. **422**, 55 (2000).
[5] H. Djeridi, C. Gabillet, and J.-Y. Billard, C. R. Mec. **330**, 113 (2002).
[6] H. Djeridi, C. Gabillet, and J.-Y. Billard, Phys. Fluids **16**, 128 (2004).
[7] S. S. S. Yim, M. Y. A. Lo, N. Titchener-Hooker, and P. Ayazi Shamlou, Bioprocess Eng. **19**, 221 (1998).
[8] W. S. Edwards, S. R. Beane, and S. Varma, Phys. Fluids A **3**, 1510 (1991).
[9] A. Davey, J. Fluid Mech. **14**, 336 (1962).
[10] S. T. Wereley and R. M. Lupetow, Phys. Fluids **11**, 328 (1999).